Available online at www.sciencedirect.com
SCIENCE DIRECT®
Journal of Solid State Chemistry 174 (2003) 80–86
JOURNAL OF SOLID STATE CHEMISTRY
http://elsevier.com/locate/jssc

Formation, sintering, and electrical conductivity of perovskite $Sm(Cr_{1-x}Mg_x)O_3$ ($0 \leqslant x \leqslant 0.23$) prepared by the hydrazine method

Ken Hirota, Miyako Io, Hiroshi Hatta, Masaru Yoshinaka, and Osamu Yamaguchi*

Department of Molecular Science and Technology, Faculty of Engineering, Doshisha University, Kyo-Tanabe, Kyoto 610-0321, Japan

Received 21 October 2002; received in revised form 1 March 2003; accepted 22 March 2003

Abstract

The presence of $SmCrO_4$ is experimentally established. In Mg^{2+}-substituted $SmCrO_3$, single-phase perovskite $Sm(Cr_{1-x}Mg_x)O_3$, where $x = 0$–0.23, are formed at $\sim$830°C by decomposition of $Sm(Cr_{1-x}Mg_x)O_4$ which crystallizes at 530–570°C from amorphous materials prepared by the hydrazine method. $Sm(Cr_{1-x}Mg_x)O_3$ solid solution powders consisting of submicrometer-size particles are sinterable; dense materials can be fabricated by sintering for 2 h at 1700°C in air. The relative densities, grain sizes, and electrical conductivities increase with increased Mg^{2+} content. $Sm(Cr_{0.77}Mg_{0.23})O_3$ materials exhibit an excellent direct current electrical conductivity of $2.2 \times 10^3\,S\,m^{-1}$ at 1000°C.

Keywords: Samarium; Chromite; Perovskite; Solid solution; Hydrazine; Electrical conductivity

1. Introduction

Refractory ABO_3 perovskite materials show relatively high electrical conductivities at elevated temperatures by substitution of either A or B sites with acceptor- or donor-type cations. Consequently, there has been considerable interest in them as high-temperature electrochemical devices. In $ACrO_3$ (A = La, Y, Nd and Sm) perovskite system, many investigations have been focussed on pure and doped materials of the former two. Little attention has been given to the sintering and electrical conductivity of the last two, especially in $SmCrO_3$. Pure $SmCrO_3$ has been prepared by a solid-state reaction [1] and a combustion synthesis [2,3]. Schneider et al. [1] studied the solid-state reaction of an equimolar mixture between Sm_2O_3 and Cr_2O_3 and reported that single-phase $SmCrO_3$ was obtained when heated at 1600°C. Combustion synthesis resulted in the formation of $SmCrO_3$ at very low temperatures. Kingsley and Pederson [2] prepared $SmCrO_3$ powders with the crystallite size of $\sim$30 nm by the exothermic redox decomposition of ammonium dichromate, samarium nitrate, and glycine mixtures at $\sim$175°C. Moreover, $SmCrO_3$ powders with fine particles of $\sim$0.1 μm were prepared by the combustion of corresponding metal nitrates and tetraformal trisazine ($C_4H_{16}N_6O_2$) in a few minutes at $\sim$425°C under ambient conditions [3].

Unfortunately, this compound, as well as other lanthanide chromites, shows poor sinterability and is very difficult to densify under atmospheric conditions. Tripathi and Lal [4] studied the AC electrical conductivity σ_{AC} of $SmCrO_3$ materials with the relative density of $\sim$67% and reported that the corrected σ_{AC} value (as 100% density sample) was as low as $2.1 \times 10^{-1}\,S\,m^{-1}$ at 727°C and 1 kHz. This value was lower in comparison with that of the direct current (DC) electrical conductivity σ_{DC} of $LaCrO_3$ ($5.1 \times 10^{1}\,S\,m^{-1}$ at 727°C) [5] and $YCrO_3$ ($5.0 \times 10^{1}\,S\,m^{-1}$ at 727°C) [6]. Two heating steps have been required for the fabrication of dense $LaCrO_3$ and $YCrO_3$ materials with high electrical conductivity [5,6]: (i) sintering under reduced pressure and (ii) annealing in air in order to fully oxidize the samples. The results suggest that the fabrication of dense $SmCrO_3$ materials by sintering in air will result in the increase in electrical conductivities.

A new powder preparation method using hydrazine monohydrate was recently developed in some systems [7,8]. In the present study, we tried to apply the same method to obtain reactive $SmCrO_3$ and

*Corresponding author. Fax: +81-774-65-6849.
E-mail address: khirota@mail.doshisha.ac.jp (O. Yamaguchi).

0022-4596/03/$ - see front matter © 2003 Elsevier Science (USA). All rights reserved.
doi:10.1016/S0022-4596(03)00178-6

Table 1
Chemical compositions of starting powders and characteristics of $Sm(Cr_{1-x}Mg_x)O_3$ materials sintered for 2 h at 1700°C in air

Sample	x in $Sm(Cr_{1-x}Mg_x)O_3$	Bulk and relative densities ($Mg\,m^{-3}$, %)	Grain size G_s (μm)	Activation energy E_a (eV)	Electrical conductivity σ at 1000°C ($S\,m^{-1}$)
A	0	6.81 (92.4)	1.2	0.26	1.6×10^2
B	0.05	6.86 (93.7)	3.0	0.24	4.0×10^2
C	0.10	6.90 (94.8)	4.5	0.24	9.6×10^2
D	0.15	6.94 (96.0)	6.4	0.23	1.4×10^3
E	0.20	6.99 (97.2)	7.0	0.22	1.9×10^3
F	0.23	7.02 (98.0)	7.5	0.22	2.2×10^3
G	0.25	—	—	—	—
H	0.30	—	—	—	—

$Sm(Cr_{1-x}Mg_x)O_3$ (substitution for the Cr site) powders. Single-phase perovskite compounds $Sm(Cr_{1-x}Mg_x)O_3$, where $x = 0-0.23$, were found to form at low temperatures by decomposition of $Sm(Cr_{1-x}Mg_x)O_4$ which crystallized from amorphous materials. Dense materials could be fabricated without any control of oxygen pressure. The present paper deals with the formation, sintering, and electrical conductivity of such $Sm(Cr_{1-x}Mg_x)O_3$.

2. Experimental procedure

Eight compositions, denoted A through H, were chosen for this study (Table 1). Samarium chloride ($SmCl_3\cdot6H_2O$, 99.9% pure), chromium chloride ($CrCl_3\cdot6H_2O$, 99.9% pure), magnesium chloride ($MgCl_2\cdot6H_2O$, 99.9% pure), and hydrazine monohydrate ($(NH_2)_2\cdot H_2O$) were used as starting materials. Aqueous solutions of the first and second chlorides and the third chloride were adjusted in concentrations of 0.5 and 0.1 mol L^{-1}, respectively, by dissolving in distilled water. An appropriate amount of hydrazine monohydrate (pH 12) was introduced into a five-necked flask equipped with a reflux condenser, a dropping funnel, a stirring rod, a thermometer and a thermocontroller. A mixed solution (pH 2) corresponding to each composition was added dropwise, with stirring, to the hydrazine at room temperature. During this process, another hydrazine monohydrate was dropped to the solution to keep their pH value constant (11.5). Then, the resulting suspension was heated for 2 h at 80°C to complete the reaction. The product was separated from the suspension by centrifugation, washed more than 10 times in hot water to remove adsorbed hydrazine and chloride ions (tested by adding a $AgNO_3$ solution), and dried at 120°C under reduced pressure.

Differential thermal analysis (DTA) and thermogravimetry (TG) were performed in air at a heating rate of 10°C min^{-1}; α-Al_2O_3 was used as the reference in DTA. The as-prepared powders and specimens, obtained from DTA runs after cooling, were examined by X-ray diffraction (XRD, Cu$K\alpha$) equipped with monochromator under a goniometer-scanning-speed of 0.25° min^{-1}. Interplanar spacings were measured with the aid of an internal standard of high-purity Si, and unit-cell values were determined by a least-squares refinement. Powders were observed by transmission electron microscopy (TEM).

Before sintering calcined powders were pressed into pellets at 196 MPa and then isostatically cold-pressed at 342 MPa. The green compacts (diameter $\varnothing\sim13$ mm and thickness $h\sim4$ mm) were sintered for 2 h at 1700°C in air. Bulk densities after polishing with diamond paste (nominal size 1–3 μm) were determined by the Archimedes method. Scanning electron microscopy (SEM) was used for microstructural observations. DC electrical conductivity σ_{DC} was measured from 400°C to 1000°C by the van der Pauw method [9] using the samples with four platinum electrodes. Platinum leads (diameter $\varnothing$ 0.2 mm) were fixed onto the disk-shaped specimen (diameter $\varnothing\sim11$ mm and thickness $h\sim1$ mm) with platinum paste and then heated for 1 h at 1100°C. Each measuring run was performed in air.

3. Results and discussion

3.1. Formation of pure $SmCrO_3$

As-prepared powder A, consisting of aggregates with ultra-fine particles (<10 nm), was amorphous to X-ray. Fig. 1(a) shows a DTA curve of the as-prepared powder A. Two successive endothermic peaks up to ~300°C are due to the release of adsorbed water and hydrated water. A sharp exothermic peak was observed at 530–570°C. As will be described, this was found to result from the crystallization of $SmCrO_4$. In addition, the curve revealed an endothermic peak resulting from decomposition of $SmCrO_4$ ($SmCrO_4\rightarrow SmCrO_3+1/2\cdot O_2$) at 825–890°C. Thermogravimetric data showed a weight decrease of 6.01% in this temperature range as shown in Fig. 1(b); this corresponds to the decrease of $1/2\cdot O_2$ per $SmCrO_4$ (theoretical value 6.007%).

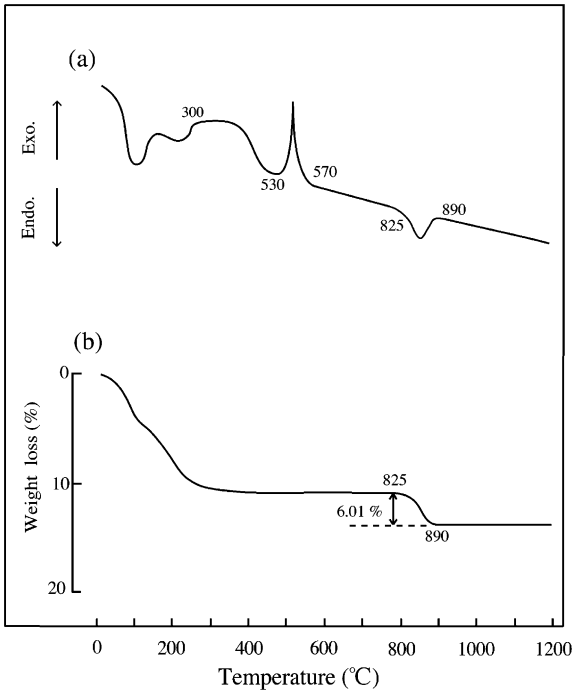

Fig. 1. (a) DTA and (b) TG curves for as-prepared powder A.

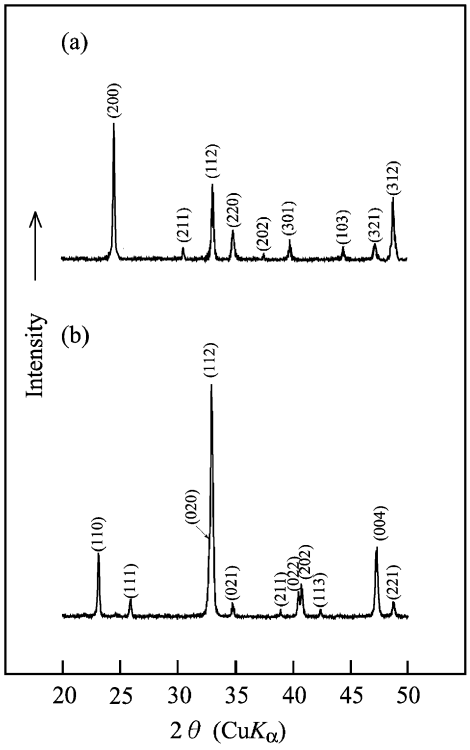

Fig. 2. X-ray diffraction patterns for (a) $SmCrO_4$ (tetragonal) and (b) $SmCrO_3$ (orthorhombic).

No significant change in structure was recognized up to 520°C. After the exothermic peak (580°C), the specimen showed a similar XRD pattern to that of $YCrO_4$ [10] and $NdCrO_4$ [11] as shown in Fig. 2(a). Buisson et al. [12] expected the presence of $SmCrO_4$ from data simulated on the basis of the $ZrSiO_4$ [13] structure. Table 2 shows XRD data for the sample heated for 1 h at 700°C. All diffraction lines could be indexed as a tetragonal unit cell with $a = 0.7250 \pm 0.0003$ nm and $c = 0.6356 \pm 0.0002$ nm, agreeing with crystallographical data ($a = 0.7251$ nm and $c = 0.6356$ nm) [14]. Thus, the presence of $SmCrO_4$ was experimentally established. Only well-crystallized $SmCrO_4$ were observed up to 820°C.

Table 2
X-ray diffraction data for $SmCrO_4$

d_{obs} (nm)	d_{calc} (nm)	I/I_o	Reference [15]		
			$h\,k\,l$	d(nm)	I/I_o
0.363	0.3625	100	2 0 0	0.36255	100
0.289	0.2888	7	2 1 1	0.28885	8.1
0.270	0.2701	69	1 1 2	0.27012	63.0
0.256	0.2563	13	2 2 0	0.25636	18.6
0.239	0.2390	4	2 0 2	0.23898	3.0
0.226	0.2259	14	3 0 1	0.22592	10.6
0.204	0.2034	7	1 0 3	0.20336	6.3
0.1917	0.19172	6	3 2 1	0.19174	8.4
0.1860	0.18594	36	3 1 2	0.18595	43.0
0.1813	0.18126	10	4 0 0	0.18127	11.6
0.1774	0.17737	3	2 1 3	0.17737	3.0
0.1695	0.16948	2	4 1 1	0.16949	2.0
0.1621	0.16212	12	4 2 0	0.16214	9.1
—	—	—	3 0 3	0.15932	1.3
0.1589	0.15891	6	0 0 4	0.15890	2.6
—	—	—	4 0 2	0.15748	0.2
0.1505	0.15051	6	3 3 2	0.15052	10.9
—	—	—	3 2 3	0.14586	1.0
0.1455	0.14554	5	2 0 4	0.14554	7.2
—	—	—	4 2 2	0.14443	0.1
0.1414	0.14137	3	5 0 1	0.14139	3.0
0.1353	0.13532	5	4 1 3	0.13532	1.8
0.1350	0.13506	7	2 2 4	0.13506	6.5
$a = 0.7250$ and $c = 0.6356$ nm			$a = 0.7251$ and $c = 0.6356$ nm		

The specimens >900°C gave the characteristic XRD pattern of $SmCrO_3$ (Fig. 2(b)) [15]. The results indicate that $SmCrO_4$ decomposed into $SmCrO_3$ and $1/2 \cdot O_2$ at 825–890°C. The crystal structure of $SmCrO_3$ had an orthorhombic unit cell with $a = 0.53696 \pm 0.00002$ nm, $b = 0.54948 \pm 0.00002$ nm, and $c = 0.76489 \pm 0.00003$ nm which were in good agreement with previous data ($a = 0.536970$ nm, $b = 0.549470$ nm, and $c = 0.764890$ nm) [15].

Fig. 3 shows TEM photographs of $SmCrO_3$ powders heated to various temperatures, indicating thin necklace-like morphology. Fine particles (~60 nm) were observed in powders at 900°C. The particles grew up to ~90 nm (1100°C) and ~130 nm (1300°C) with increased temperature.

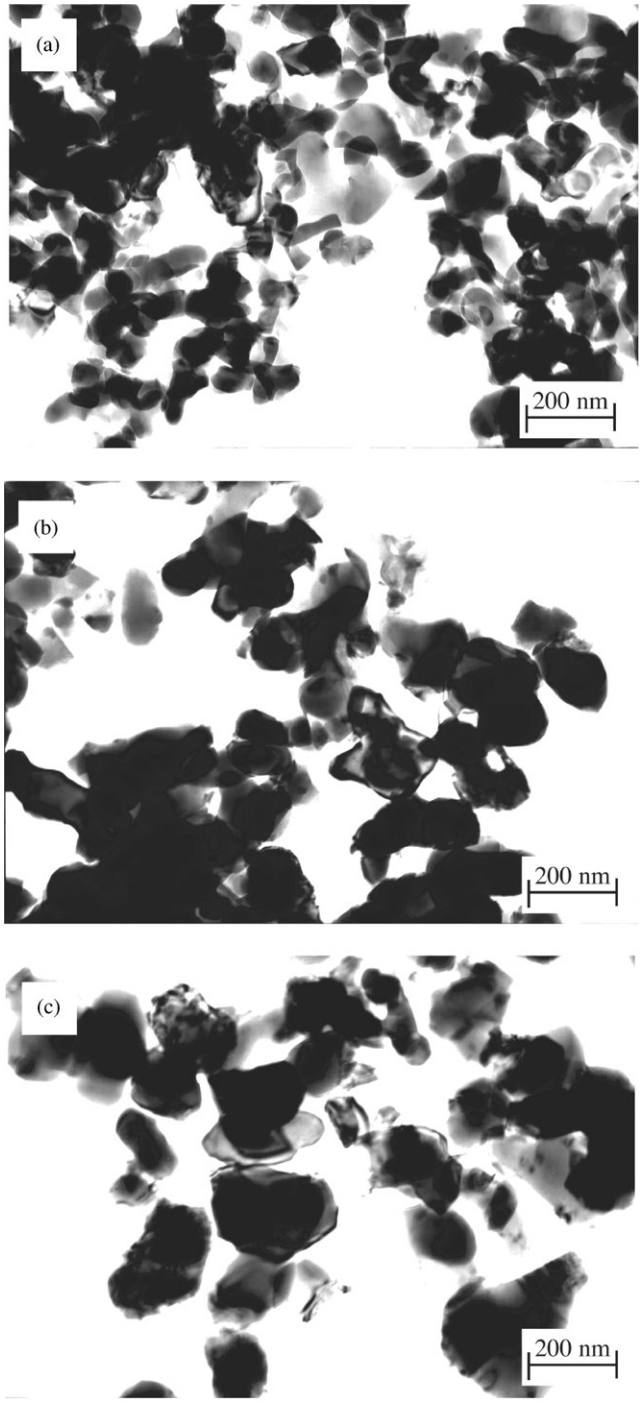

Fig. 3. TEM photographs of $SmCrO_3$ powders heated to (a) 900°C, (b) 1100°C, and (c) 1300°C.

3.2. Formation of $Sm(Cr_{1-x}Mg_x)O_3$

The as-prepared powders B through H were also amorphous. They all, as well as the powder A, revealed exothermic and endothermic peaks corresponding to the crystallization of $Sm(Cr_{1-x}Mg_x)O_4$ and decomposition of this into $Sm(Cr_{1-x}Mg_x)O_3$,[1,2] respectively. The former peaks decreased gradually in height with increased Mg^{2+} content from B to F. For powders G and H, the XRD lines corresponding to Sm_2O_3 [18] were present in the specimens after heating at 595°C. The specimens heated at temperatures above the endothermic peaks were mixtures of $Sm(Cr_{1-x}Mg_x)O_3$ and Sm_2O_3. Compositional changes result in a significant variation in cell dimensions. Fig. 4 shows the lattice parameters for $Sm(Cr_{1-x}Mg_x)O_3$ obtained by heating for 1 h at 950°C. Up to 23 mol% Mg^{2+} content the values of a, b, and c increased linearly: a $(0.53696 \pm 0.00002 \rightarrow 0.53752 \pm 0.00002\,\text{nm})$, b $(0.54948 \pm 0.00002 \rightarrow 0.54993 \pm 0.00002\,\text{nm})$ and c $(0.76489 \pm 0.00003 \rightarrow 0.76544 \pm 0.00003\,\text{nm})$. This result indicates that larger Mg^{2+} with an ionic radius of 0.0720 nm [19] was substituted for octahedrally coordinated smaller Cr^{3+} (0.0615 nm)/Cr^{4+} (0.0550 nm) [19] in the perovskite structure. This gives abundant evidence for formation of complete solid solutions. Thus, single-phase $SmCrO_3$ solid solutions containing Mg^{2+} up to 23 mol% are found to be formed by the hydrazine method.

3.3. Sintering and microstructure

The as-prepared powders A through F were calcined for 1 h at 1000°C. The calcined powders (~0.1 μm) were sintered as already described. The materials consisted of only the perovskite phase. Table 1 shows the bulk and relative densities of $Sm(Cr_{1-x}Mg_x)O_3$ materials. The relative densities were estimated using theoretical densities calculated from molecular weights, the number of chemical formula units per unit cell ($Z = 4$) [15], Avogadro's number, and lattice parameters. Pure $SmCrO_3$ materials had a bulk density of 6.81 $Mg\,m^{-3}$, corresponding to 92.4% of theoretical density (7.356 $Mg\,m^{-3}$) [15].[3] The relative densities increased with increased Mg^{2+} content. Finally, $Sm(Cr_{0.77}Mg_{0.23})O_3$ materials had 98.0% of theoretical. Fig. 5 shows SEM photographs for fracture surfaces of several materials. Average grain sizes were determined by the intercept method [20]. As shown in Table 1, they increased from 1.2 to 7.5 μm with increased Mg^{2+}

[1] Due to much difficulty in determination of oxygen content in both powders and materials heated at high temperatures, Mg-doped samarium chromites were expressed as $Sm(Cr_{1-x}Mg_x)O_3$ as the same manner adopted in many previous studies investigating the transport properties of low-valent cation doped rare-earth chromites such as $(Sm_{1-x}Ca_x)(Cr_{1-y}Cu_y)O_3$ [16].

[2] The evidence that Mg^{2+} was substituted into the B site was confirmed by X-ray Rietveld analysis [17]; the R_{wp} (R-weighted pattern) for Sample A ($x = 0$) and F ($x = 0.23$) gave the smallest values of 11.68% and 12.09%, respectively, when the distribution of chromium/magnesium ions was presumed to be 1/0 and 0.77/0.23 on the B site of the perovskite structure.

[3] Sintering for 4 h at 1600°C gave the materials with the relative densities of <90%.

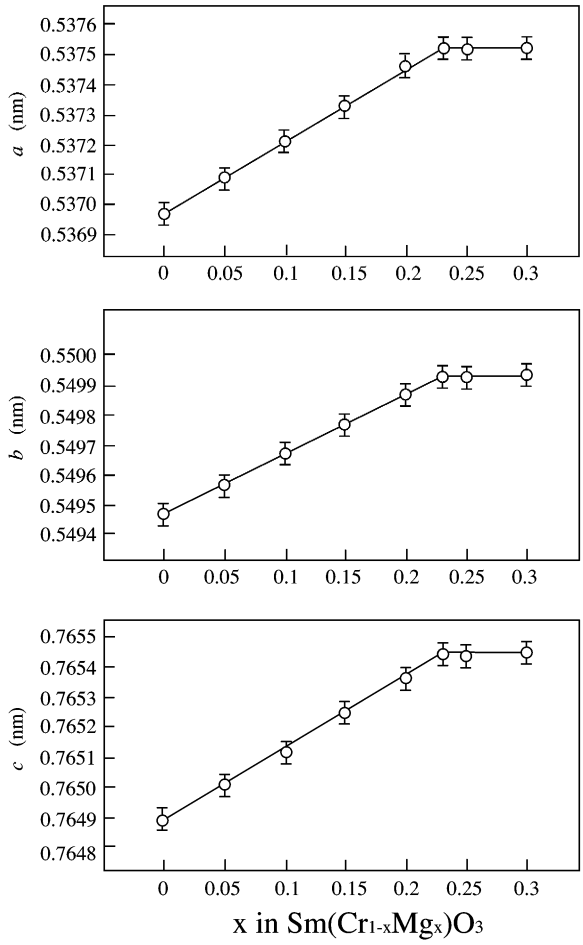

Fig. 4. Lattice parameters of Mg^{2+}-doped $SmCrO_3$ obtained by heating for 1 h at 900°C.

content. These results suggested that the substitution of Mg^{2+} on Cr^{3+} site induced a small amount of oxygen defects in the crystals, which enhanced the densification and grain growth during sintering. Note that the dense materials could be obtained by sintering in air. This result indicates that the present powders were sinterable.

3.4. Electrical conductivity

The temperature dependence of electrical conductivity (σ) of $SmCrO_3$ materials in a plot of Log(σT) against reciprocal absolute temperature $1/T$ is shown in Fig. 6 and compared with that of σ which gave the best data for $LaCrO_3$ [5] and $YCrO_3$ [6] materials. The latter two orthochromites were fabricated by sintering (under low oxygen partial pressure) powders prepared by the liquid-mix process [21] and then annealed in air at 1527°C for 48 h in order to be fully oxidized. On the other hand, a conventional ceramic processing for $SmCrO_3$ materials resulted in a low bulk value of AC electrical conductivity σ_{AC} 2.1×10^{-1} S m^{-1} at 727°C and 1 kHz [4]. This value, corresponding to that of fully densified materials, was

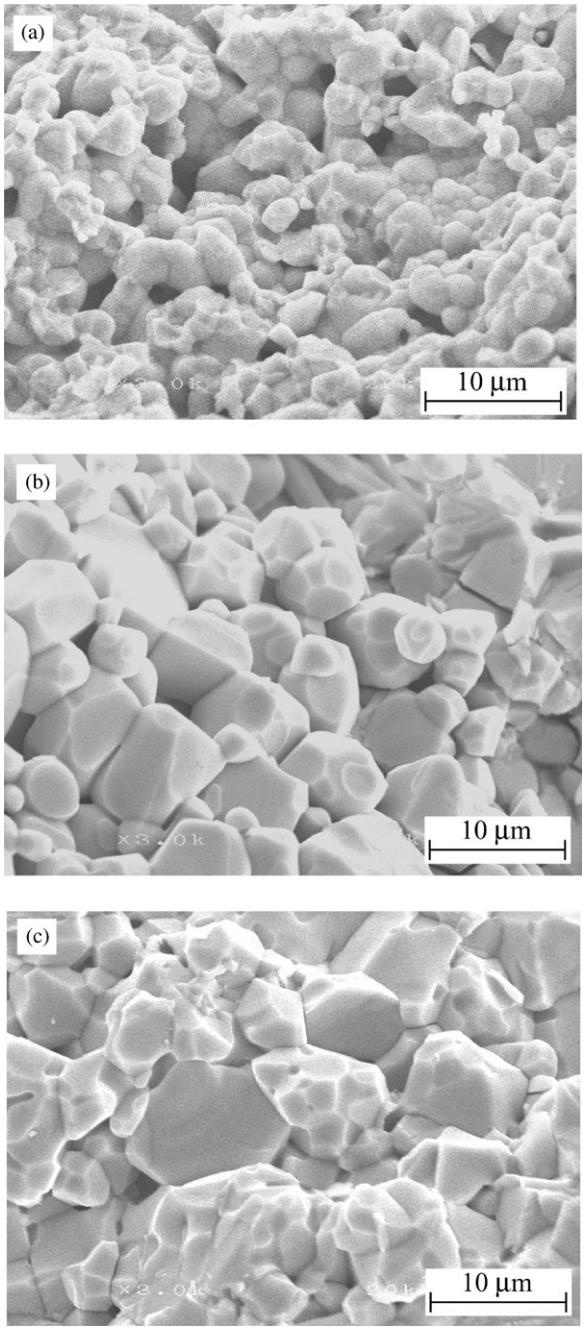

Fig. 5. SEM photographs for fracture surfaces of (a) $SmCrO_3$, (b) $Sm(Cr_{0.85}Mg_{0.15})O_3$, and (c) $Sm(Cr_{0.77}Mg_{0.23})O_3$ materials.

thought to be independent on the applied signal frequency [4]. Their Log(σT) value of 2.33 Sm^{-1}K at 727°C was much smaller than that ($\sim$5.05 Sm^{-1}K) for the present $SmCrO_3$ materials (Fig. 6(a)). These results indicate that the difference in electrical conductivity has been caused by the rare-earth ion, depending much on the fabrication processing.

Earlier studies on undoped $LaCrO_3$ and $YCrO_3$ indicated that they were p-type semiconductors and their electrical conductivities were essentially due to the 3-*d* band of the Cr ions through the formation of cation

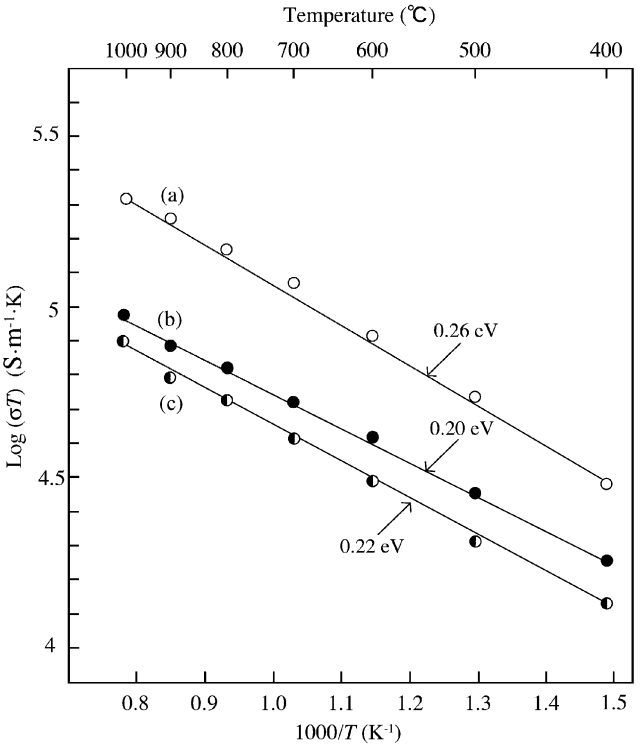

Fig. 6. Log(σT) for (a) $SmCrO_3$, (b) $LaCrO_3$, (c) $YCrO_3$ materials as a function of $1/T$.

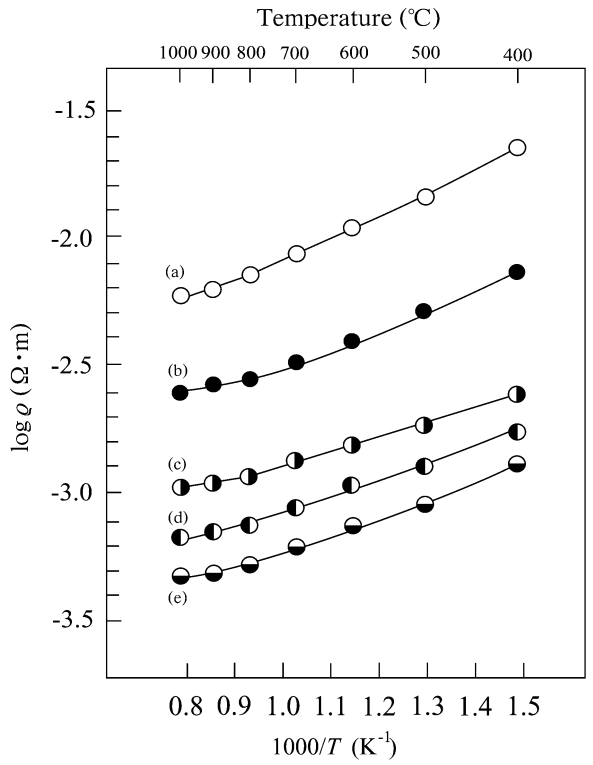

Fig. 7. Log(ρ) for (a) $SmCrO_3$, (b) $Sm(Cr_{0.95}Mg_{0.05})O_3$, (c) $Sm(Cr_{0.90}Mg_{0.10})O_3$, (d) $Sm(Cr_{0.85}Mg_{0.15})O_3$, and (e) $Sm(Cr_{0.77}Mg_{0.23})O_3$ materials as a function of $1/T$.

vacancies [22,23]. In addition, in all rare-earth orthochromites small polarons seemed to be responsible for the conduction [23]. In this study the p-type semiconductivity of $SmCrO_3$-based materials thus fabricated was confirmed by testing Seebeck effect. In Fig. 6, the conductivities of pure rare-earth chromites are well represented by the function of $(1/T)\exp(-E_a/kT)$, where E_a the activation energy, and k the Boltzmann constant. The value of $1.6\times10^2\,S\,m^{-1}$ was obtained at 1000°C. This value was higher >2 times than that of $LaCrO_3$ ($70.3\,S\,m^{-1}$) and $YCrO_3$ ($61.1\,S\,m^{-1}$) materials. Thus, the electrical conductivity of $SmCrO_3$ must be originated from the 3*d*-electrons. The activation energy was determined to be 0.26 eV. However, a plot of Log(ρ) vs. $1/T$ as shown in Fig. 7, where ρ is the electrical resistivity of $SmCrO_3$-based materials, exhibited a nonlinear relationship between them.

Fig. 8 shows the temperature dependence of electrical conductivities of several $Sm(Cr_{1-x}Mg_x)O_3$ materials. Anikina et al. [16] studied the transport properties of sintered $Sm_{1-x}Ca_xCr_{1-y}Cu_yO_3$ ($x=0.2$, $y=0-0.20$ and $x=0.3$, $y=0-0.20$) and showed that the linear dependence of Log(σT) vs. $1/T$ for the materials measured at 500–1000°C was characteristic of the small polaron hopping transport which was often observed in chrome-based perovskites [24,25]. In this study, similar results were also obtained; the σ data at 1000°C are

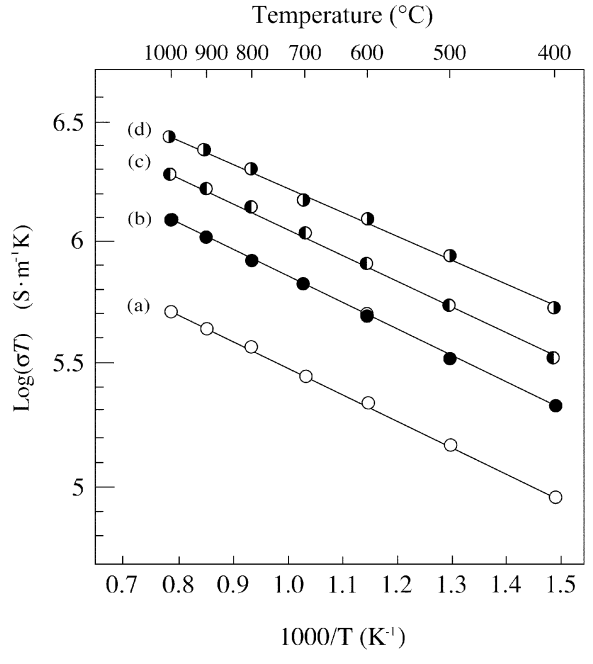

Fig. 8. Log(σT) for (a) $Sm(Cr_{0.95}Mg_{0.05})O_3$, (b) $Sm(Cr_{0.90}Mg_{0.10})O_3$, (c) $Sm(Cr_{0.85}Mg_{0.15})O_3$, and (d) $Sm(Cr_{0.77}Mg_{0.23})O_3$ materials as a function of $1/T$.

given in Table 1. Among these materials, $Sm(Cr_{0.77}Mg_{0.23})O_3$ showed the value of $2.2\times10^3\,S\,m^{-1}$, in which the magnitudes of σ are comparable to those of

Sr^{2+}- and Ca^{2+}-substituted $LaCrO_3$ [7,20,22]. Our structural[4] and electrical[5] data were applied to a model for hopping transport [26]. Hole mobility μ_p in the highest conductivity material was calculated to be $3.37 \times 10^{-6}\,m^2\,V^{-1}\,s^{-1}$. Then, ω_0 the frequency of a characteristic optical phonon was determined to be $4.67 \times 10^{13}\,s^{-1}$, which value satisfied such condition as $\omega_0(h/2\pi) \ll kT$, where h is the Planck constant, k the Boltzmann constant, and T the absolute temperature. This condition has been required for small-polaron hopping mechanism [27]. Thus an increase in the conductivity up to the Mg^{2+}-substituted level of $x \leqslant 0.23$ must be attributed to the formation of Cr^{4+} ions as a result of charge compensation caused by the hopping polarons between Cr^{3+} and Cr^{4+} ions.

4. Conclusion

The hydrazine method results in the formation of $SmCrO_4$ with the tetragonal structure of $a = 0.7250 \pm 0.0003$ nm and $c = 0.6356 \pm 0.0002$ nm. Perovskite $SmCrO_3$ is formed at $\sim 830°C$ by decomposition of $SmCrO_4$. In the $Sm(Cr_{1-x}Mg_x)O_3$ solid solutions, an extensive region up to $x = 0.23$ occurs in which the perovskite structure is present as a single phase. $Sm(Cr_{1-x}Mg_x)O_3$ powders are highly sinterable. Dense sintered materials can be fabricated without any control of oxygen pressure. Electrical conductivity increases with increased Mg^{2+} content. Materials with the composition of $x = 0.23$ exhibit an excellent electrical conductivity at elevated temperatures.

Acknowledgments

This work was supported by a grant to Research Center for Advanced Science and Technology at Doshisha University from the Ministry of Education, Japan.

[4] The equilibrium lattice parameter $\langle a \rangle = (abc)^{1/3} = 0.60936 \pm 0.00003$ nm was calculated from the measured lattice parameters ($a = 0.53752 \pm 0.00002$ nm, $b = 0.54993 \pm 0.00002$ nm, and $c = 0.76544 \pm 0.00003$ nm).

[5] The concentration of charge carrier (hole) $p = 4.07 \times 10^{27}\,m^{-3}$ and the activation energy $E_a = 0.22$ eV were used.

References

[1] S.J. Schneider, R.S. Roth, J.L. Waring, J. Res. Natl. Bur. Stand. 65A (1961) 345–374.
[2] J.J. Kingsley, L.R. Pederson, Mater. Lett. 18 (1993) 89–96.
[3] S.S. Manoharan, K.C. Patil, J. Solid State Chem. 102 (1993) 267–276.
[4] A.K. Tripathi, H.B. Lal, J. Mater. Sci. 17 (1982) 1595–1609.
[5] D.P. Karim, A.T. Aldred, Phys. Rev. B 20 (1979) 2255–2263.
[6] W.J. Weber, C.W. Griffin, J.L. Bates, J. Am. Ceram. Soc. 70 (1987) 265–270.
[7] K. Ishida, K. Hirota, O. Yamaguchi, J. Am. Ceram. Soc. 77 (1994) 1391–1395.
[8] T. Tachiwaki, M. Yoshinaka, K. Hirota, T. Ikegami, O. Yamaguchi, Solid State Commun. 119 (2001) 603–606.
[9] van der Pauw, Philips Res. Rep. 13 (1958) 1–9.
[10] Powder diffraction file, Card No. 16-249. Joint committee on powder diffraction standards, Swarthmore, PA, 1974.
[11] Powder diffraction file, Card No. 16-880. Joint committee on powder diffraction standards, Swarthmore, PA, 1974.
[12] G. Buisson, F. Bertaut, J. Mareschal, Compt. Rend. 259 (1964) 411–413.
[13] Powder Diffraction File, Card No. 6-266, American Society for testing and materials, Philadelphia, PA, 1967.
[14] Powder Diffraction File, Card No. 74-1245 (PDF#74-1245), Joint committee on powder diffraction standards, Swarthmore, PA.
[15] Powder Diffraction File, Card No. 39-262, Joint committee on powder diffraction standards, Swarthmore, PA, 1993.
[16] E.L. Anikina, V.I. Zemtsov, E.I. Burmakin, Inorg. Mater. 36 (2000) 74–76.
[17] F. Izumi, M. Mitomo, Y. Bando, J. Mater. Sci. 19 (1984) 3115–3120.
[18] Powder Diffraction File, Card No. 42-1461, Joint committee on powder diffraction standards, Swarthmore, PA, 1993.
[19] R.D. Shannon, C.T. Prewitt, Acta Crystallogr. B 25 (1969) 925–946.
[20] S. Bajo, Anal. Chem. 50 (1978) 649–651.
[21] M.P. Pechini, US Pat. No. 3330697, July 1967.
[22] D.B. Meadowcroft, in: T. Gray (Ed.), International Conference on Strontium Containing Compounds, Atlantic Research Institute, Halifax, Canada, 1973, pp. 119–136.
[23] G.V. Subba Rao, B.M. Wanklyn, C.N.R. Rao, J. Phys. Chem. Solids 32 (1971) 345–358.
[24] K.P. Bansal, S. Kumari, B.K. Das, G.C. Jain, J. Mater. Sci. 18 (1983) 2095–2100.
[25] K. Gaur, S.C. Varma, H.B. Lal, J. Mater. Sci. 23 (1988) 1725–1728.
[26] T. Holstein, Ann. Phys. (Paris) 8 (1959) 325–342.
[27] H. Böttger, V.V. Bryksin, Phys. Stat. Sol. B 78 (1976) 9–56.